Laser Physics, Vol. 14, No. 1, 2004, pp. 1–14.

Simulation of KrCl (222 nm) and XeCl (308 nm) Excimer Lamps with Kr/HCl(Cl_2) and Xe/HCl(Cl_2) Binary and Ne/Kr/Cl_2 Ternary Mixtures Excited by Glow Discharge

A. M. Boichenko and S. I. Yakovlenko

General Physics Institute, Russian Academy of Sciences, ul. Vavilova 38, Moscow, 119991 Russia

e-mail: syakov@kapella.gpi.ru, kindep@kapella.gpi.ru

Received October 15, 2002

Abstract—Based on the kinetic models of XeCl and KrCl active media in Kr/HCl(Cl_2), Xe/HCl(Cl_2), and Ne/Kr/Cl_2 mixtures, the simulation of XeCl and KrCl excimer lamps pumped by glow discharge is carried out. The optimum compositions of the mixtures are determined. The results obtained are compared with the available experimental data.

1. INTRODUCTION

Excimer lamps with rare gas/halogen exciplex molecules are sources of spontaneous radiation, whose main advantage over explosive and high-current-discharge lamps is a relatively narrow (a few nanometers) emission band. Such sources deliver high-intensity radiation, needed, for example, for stimulating photochemical and photophysical processes, such as photolytic processing of metal, dielectric, and semiconductor layers and surface cleaning. Excimer lamps can also be used to destroy hazardous organic substances and harmful bacteria. The possibility of substituting excimer lamps for ecologically unsafe mercury lamps is discussed. One can use excimer lamps in biology, medicine, and ecology.

Excimer lamps can be excited using barrier discharge [1–8], pulsed volume discharge [9–12], a hard ionizer (with beams and nuclear fragments) [13–17], capacitive discharge [18–20], spark discharge [21], microwave radiation [22–26], shock wave (Voitenko lamps) [27–29], gas-dynamic flows [30–32], inductive discharge [33, 34], etc. Lamps excited by glow discharge [19, 35–44] exhibit both high mean power and high efficiency of the discharge energy transformation into light.

In the first related works [35, 36], the efficiencies were relatively low (about 1%). In [37, 38], the efficiency was increased to more than 10%, as proven in [38–44]. High-power glow-discharge lamps (about 10 W per cm of lamp length) with high efficiencies were reported in [45–48].

In continuation of [41, 42], we describe in this work the emission characteristics of excimer lamps with rare gas halides pumped by glow discharge. In the aforementioned works, one can find the analysis of the fundamental processes in the glow discharge plasma of excimer lamps and the corresponding estimates. However, numerical simulation of the lamps is missing. Based on the results of the analysis, a conclusion has been drawn regarding the possibility of high efficiencies of such light sources. Below, we present the results of a detailed simulation.

2. KINETIC MODEL

Kinetic models. We construct kinetic models for Ne/Xe/HCl and Ne/Kr/HCl mixtures. The models take into account the following reagents: Ne^+, Ne_2^+, $NeKr^+$, $NeXe^+$, Kr^+, Kr_2^+, Xe^+, Xe_2^+, Cl^+, Cl_2^+, H^+, H_2^+, HCl^+, and Cl^+ ions; Ne*, Kr*, Xe*, Cl*, and H* lower electron states of atoms; Ne_2^*, Kr_2^*, Xe_2^*, NeKr*, NeXe*, NeKrCl*, NeCl*, Cl_2^*, Kr_2Cl^*, and Xe_2Cl^* lower electron excited states of molecules; Ne**, Kr**, Xe**, Kr_2^{**}, and Xe_2^{**} higher excited states; Ne, Kr, Xe, H, and Cl atoms; HCl, Cl_2, H_2, and XeCl(X) ground-state molecules; HCl(v = 1, 2) and H_2(v = 1) molecules in lower excited vibrational states; exciplex molecules in the states KrCl(*B*, *C*), XeCl(*B*, *C*), and KrCl(*D*); and free electrons.

The kinetic models are based on the results of active medium simulation for a few lasers (in particular, a XeCl laser) and a KrCl excimer lamp [7, 12, 49–51]. We solve a system of nonlinear ordinary differential equations describing the time evolution of the concentrations of the above reagents using PLAZER computer codes [51, 52]. We assume spatial homogeneity of the concentrations of the reagents. The numerical simulation takes into account various processes: ionization by field-heated electrons, escape of electrons owing to the ambipolar diffusion, dissociative recombination, three-body recombination (in particular, three-body recombination involving heavy particles), electron attachment to halogen molecules and atoms, etc.

We introduce an effective diffusion time to take into account the variation in the ion density N_i related to the ambipolar diffusion:

$$\left(\frac{dN_i}{dt}\right)_{diff} = -\frac{N_i}{\tau_{diff}},$$

where $\tau_{diff} = \frac{1}{D_a}\left(\frac{r}{2.4}\right)^2$, r is the tube radius, and D_a is the ambipolar diffusion coefficient of ions.

At each time moment, we simultaneously solve the kinetic equations and the equations for the electron velocity distribution function [51] in the presence of a given electric field with strength E.

Preionization. Expressions (1) and (2) (see below) represent relationships between the mean electron energy and the tube radius (see Section 3). They do not affect the electron concentration in the discharge, which depends on only a few factors, in particular, on the discharge preionization level. Discharges with different electron concentrations exhibit different current densities and radiation powers. The discharge cannot be ignited in the absence of the preionization. In a real discharge, the preionization can be caused, for example, by electron avalanche. In calculations, the preionization is homogeneous with respect to the discharge volume.

The preionization intensity depends on the preionization rate ν; so the model contains two additional equations,

$$d[Ne^+]/dt = \nu_{Ne}[Ne]$$

$$d[Xe^+]/dt = \nu_{Xe}[Xe].$$

Below, we present the neon preionization rate $\nu = \nu_{Ne}$. The relationship between the xenon and neon ionization rates is written as $\nu_{Xe} \approx 8\nu_{Ne}$. Note that, in calculations, both the power density and the discharge current linearly increase with ν increasing from 10^{-3} to 10^{-1} s^{-1}. For the binary mixtures, the preionization rate equals 10^{-3} s^{-1} (for example, this rate for pure xenon ($\nu_{Xe} \approx 8 \times 10^{-3}$ s^{-1}), corresponds to the current density of the electron beam $j = 6.8 \times 10^{-4}$ A/cm^2 and the electron energy is 100 keV) and its duration approximately equals 10 μs.

Steady-state burning of the discharge. In the simulation of the steady state corresponding to the glow discharge, we employ the following. At the given parameters of the medium, the steady-state mode is realized at a certain field strength E_{st}. If $E > E_{st}$, all atoms are ionized. In the opposite case ($E < E_{st}$), the initial seed concentration rapidly decreases down to zero. The closer the field strength to E_{st}, the longer the duration of the steady state in the absence of the sources of preionization. In simulations, we use test calculations to choose the field strength corresponding to the steady-state discharge burning. The values of various quantities calculated for the steady-state scenario are used as theoretical values characterizing the given discharge.

The fact that the steady-state mode is realized at a certain electric field strength can be interpreted in the following way. A simplified balance equation for the electron density N_e can be written as

$$\frac{dN_e}{dt} = \left(\nu(E) - \frac{1}{\tau_{diff}} - \frac{1}{\tau_{rec}}\right)N_e = 0. \quad (1)$$

Here, the first term in the right-hand side corresponds to the creation of electrons ($\nu(E)$ is the ionization rate strongly dependent on the electric field strength), the second term corresponds to the radial ambipolar diffusion of electrons, and the third term describes the recombination processes (τ_{rec} is the characteristic time of the recombination processes).

A steady state is realized when the expression in parentheses equals zero. If this expression weakly depends on the electron density, the electric field strength corresponding to the steady-state discharge weakly depends on N_e. In the case of a strong dependence on N_e, one can realize the steady state at any value of the electric field strength E by appropriately choosing the value of N_e.

The quantities $\nu(E)$ and τ_{diff} weakly depend on the electron density. In the case when the recombination processes are negligible and the discharge is diffusion-controlled, the electric field strength E_{st} corresponding to the stead-state discharge burning is given by the condition $\nu(E_{st}) = 1/\tau_{diff}$ and weakly depends on the electron density.

3. PURE RARE GASES

We test the plasma model under consideration based on a comparison of the results of calculations with the analytical and experimental results for the plasma of pure rare gases. Attention is paid mainly to the neon plasma, owing to the large amount of corresponding experimental data and better validation of the analytical results.

Steady-state electron temperature for the maxwell distribution. For the glow discharge in neon, there exists a universal dependence $T_e(pr)$ of the electron temperature in the positive column on the product of the pressure and the positive column radius [53–55]. This dependence is obtained for the diffusion-controlled discharge assuming a Maxwell distribution function of electrons in the discharge.

Indeed, in the case of the diffusion-controlled discharge, the steady-state condition (see Eq. (1)) can be represented as

$$k_i N = D_a\left(\frac{2.4}{r}\right)^2. \quad (2)$$

Here, N is the neon atomic density,

$$k = \int \sigma_i(\varepsilon)(2\varepsilon/m_e)^{1/2} f(\varepsilon) d\varepsilon$$

is the ionization rate of neon atoms, $\varepsilon = m_e v^2/2$ is the electron kinetic energy, m_e is the electron mass, and $\sigma_i(\varepsilon)$ is the ionization cross section.

In the vicinity of the threshold, the ionization cross section virtually linearly depends on the incident electron energy:

$$\sigma_i(\varepsilon) = \alpha(\varepsilon - I), \quad \varepsilon \geq I, \tag{3}$$

where I is the ionization energy and α is a constant characterizing the rate of the increase in the cross section in the near-threshold region. With allowance for the Maxwell distribution of electrons with respect to energy

$$f(\varepsilon) = f_M(\varepsilon) \equiv \frac{2\sqrt{\varepsilon}}{\sqrt{\pi} T_e^{3/2}} \exp(-\varepsilon/T_e)$$

and the linear approximation (3) of the cross section in the vicinity of the threshold, we obtain the following expression for the ionization rate:

$$\nu = k_i N = N\bar{v}\alpha T_e (I/T_e + 2)\exp(-I/T_e),$$

where $\bar{v} = \sqrt{\dfrac{8T_e}{\pi m_e}}$ is the mean electron velocity. In the case of the Maxwell distribution, the ionization rate implicitly depends on the electric field strength E via the electron temperature, which depends on the Joule heating proportional to the square of the field strength.

When the electron temperature is significantly higher than the ion temperature (which is typical of glow discharge), we have the following expression for the ambipolar diffusion coefficient:

$$D_a \approx \mu_+ T_e/e,$$

where μ_+ is the mobility of positive ions in plasma given by

$$\mu_+ = \frac{e}{M\nu_+}. \tag{4}$$

Here, ν_+ is the frequency of the ion–ion and ion–atom collisions, e is the electron charge, and M is the mass of gas particles (neon atoms). With allowance for $I \gg T_e$, we finally obtain the equation for electron temperature [53–55]:

$$\exp(I/T_e)\sqrt{\frac{T_e}{I}} = A(pr)^2, \tag{5}$$

where $A = \dfrac{\alpha}{\mu_+ p}\sqrt{\left(\dfrac{8I}{\pi m_e}\right)}\dfrac{N}{p}\left(\dfrac{1}{2.4}\right)^2$. For neon, the recommended value of this constant is $A = 4.3 \times 10^2$ (torr cm)$^{-2}$ [53]. Equation (5) was used to describe the glow discharge for a long time. For a few gases, the values of constant A were measured by Engel and Steenbeck as early as 1934 [53].

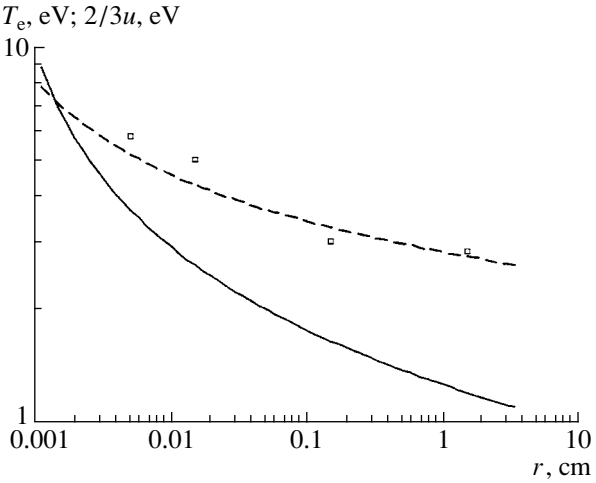

Fig. 1. T_e vs. pr for the positive column of the neon glow discharge calculated assuming Maxwell (solid line) and Druyvestein (dashed line) electron energy distribution functions. For simplicity, the curves are plotted for p = 147 torr. Dots show the results of simulation.

Equation (5) yields the dependence of T_e/I on pr. The solid curve in Fig. 1 shows this dependence for neon. For the sake of simplicity, we present the dependence $T_e(r)$ for p = 147 torr.

Steady-state electron temperature for the Druyvestein distribution. It is well known that, when the electron path is independent of energy and there is an electric field present, it is expedient to use the Druyvestein electron distribution function rather than the Maxwell electron distribution function. The condition for the constancy of the transport cross section in electron scattering is especially well satisfied for neon (for energies ranging from 1 to 100 eV, the cross section is $\sigma_{tr} = (2–3) \times 10^{-16}$ cm^2) [56]. The Druyvestein distribution can be represented as

$$f(\varepsilon) = f_D(\varepsilon) \equiv \frac{2}{\Gamma(3/4)}\left(\frac{3m_e}{M}\right)^{3/4}\sqrt{\frac{\varepsilon}{\varepsilon_0^3}}\exp\left(-\frac{3m_e}{M}\frac{\varepsilon^2}{\varepsilon_0^2}\right).$$

Here, M is the mass of a gas particle (neon atom), $\Gamma(3/4) = 1.225$, and

$$\varepsilon_0 = eE/(\sigma_{tr} N) \tag{6}$$

is the electron energy acquired at the distance $l = 1/(\sigma_{tr} N)$ between the elastic collisions in the presence of an electric field with strength E.

For the further calculations, we represent the above distribution function in terms of the variables $y = \varepsilon^2$ and $y_0 = \frac{M\varepsilon_0^2}{3m_e}$:

$$f(\sqrt{y}) = 2y^{1/4}C\exp(-y/y_0),$$

where

$$C = \frac{1}{\Gamma(3/4)y_0^{3/4}}.$$

To derive an analog of expression (5) for the Druyvestein electron distribution function, we calculate the ionization rate and express it in terms of the energy quantity analogous to temperature. Apparently, the temperature for the Druyvestein distribution is defined as two-thirds of the mean electron energy:

$$T_D = (2/3)\bar{\varepsilon} = (2/3)\int_0^\infty \varepsilon f_D(\varepsilon)d\varepsilon,$$

$$\bar{\varepsilon} = Cy_0^{5/4}\Gamma(5/4) = y_0^{1/2}\frac{\Gamma(5/4)}{\Gamma(3/4)};$$

therefore, we have

$$T_D = \beta y_0^{1/2}, \quad (7)$$

where $\beta = \frac{2\Gamma(5/4)}{3\Gamma(3/4)} \approx 0.493$. Taking into account expression (6), we express the temperature in terms of the electric field strength:

$$T_D = \beta\sqrt{\frac{M}{3m_e}}\frac{eE}{\sigma_{tr}N}.$$

Using formulas (3) and (7), we obtain the following expression for the ionization rate:

$$k_i(T_D) = \int_0^\infty \sigma_i(\varepsilon)\sqrt{2\varepsilon/m_e}f(\varepsilon)d\varepsilon$$

$$= \alpha C\left(\frac{2}{m_e}\right)^{1/2}\int_{I^2}^\infty (y^{1/2} - I)\exp(-y(\beta/T_D)^2)dy$$

$$= k_i^1(T_D) - k_i^0(T_D),$$

where

$$k_i^1(T_D) = \alpha C\left(\frac{2}{m_e}\right)^{1/2}\int_{I^2}^\infty y^{1/2}\exp(-y(\beta/T_D)^2)dy$$

$$= \alpha C\left(\frac{2}{m_e}\right)^{1/2}\left(\frac{T_D}{\beta}\right)^3\Gamma(3/2, (\beta I)^2/T_D)$$

$$= \alpha C\left(\frac{2}{m_e}\right)^{1/2}\left(\frac{T_D}{\beta}\right)^2 I\exp(-(\beta I/T_D)^2)$$

$$\times\left[1 + \frac{1}{2}\left(\frac{T_D}{\beta I}\right)^2 - \frac{1}{4}\left(\frac{T_D}{\beta I}\right)^4 + \frac{3}{8}\left(\frac{T_D}{\beta I}\right)^6 - \ldots\right].$$

Here, $\Gamma(a, b)$ is the incomplete gamma function, whose asymptotic representation is written as [57]

$$k_i^0(T_D) = \alpha C\left(\frac{2}{m_e}\right)^{1/2}\int_{I^2}^\infty I\exp(-y(\beta/T_D)^2)dy$$

$$= \alpha CI\left(\frac{2}{m_e}\right)^{1/2}\left(\frac{T_D}{\beta}\right)^2\exp(-(\beta I/T_D)^2).$$

Thus, we have

$$k_i = k_i^1(T_D) - k_i^0(T_D)$$

$$= \alpha CI\left(\frac{2}{m_e}\right)^{1/2}\left(\frac{T_D}{\beta}\right)^2\exp(-(\beta I/T_D)^2)$$

$$\times\left[\frac{1}{2}\left(\frac{T_D}{\beta I}\right)^2 - \frac{1}{4}\left(\frac{T_D}{\beta I}\right)^4 + \frac{3}{8}\left(\frac{T_D}{\beta I}\right)^6 - \ldots\right].$$

Normally, $T_D \ll I$; hence, the ionization rate is represented as

$$k_i = \frac{\alpha}{\Gamma(3/4)I}\left(\frac{1}{2m_e}\right)^{1/2}\frac{T_D^{5/2}}{\beta^{5/2}}\exp(-\beta^2 I^2/T_D^2).$$

In this case, Eq. (2) is transformed into the following equation:

$$\left(\frac{r}{2.4}\right)^2\frac{\alpha}{\Gamma(3/4)I}\left(\frac{1}{2m_e}\right)^{1/2}\frac{T_D^{5/2}}{\beta^{5/2}}\exp(-\beta^2 I^2/T_D^2)N$$

$$= D_a = \frac{\mu_+ T_D}{e}.$$

Table data regarding the ion mobility μ_+^0 are measured under certain (e.g., normal) conditions. Taking into account the inverse proportionality of the ion mobility to the collision frequency (4), we arrive at

$$\mu_+ N\sqrt{T} = \mu_+^0 N_0\sqrt{T_0}$$

and, hence,

$$\exp(\beta^2 I^2/T_D^2)\left(\frac{I}{T_D}\right)^{3/2}$$

$$= \left(\frac{r}{2.4}\right)^2\frac{e\alpha}{\Gamma(3/4)}\left(\frac{I}{2m_e}\right)^{1/2}\frac{1}{\beta^{5/2}}\frac{N^2\sqrt{T}}{\mu_+^0 N_0\sqrt{T_0}}.$$

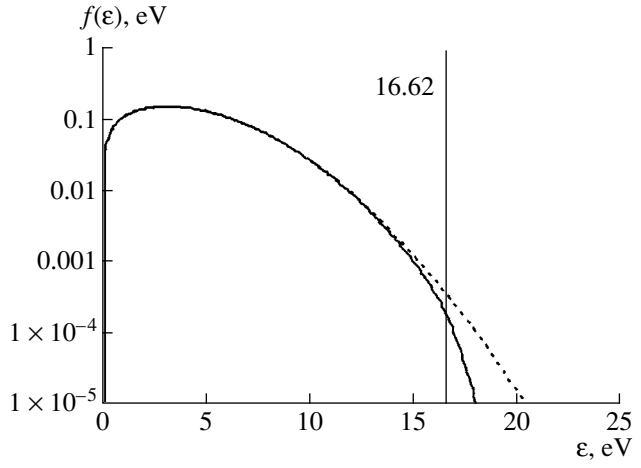

Fig. 2. Comparison of the calculated (solid line) and Druyvestein (dashed line) electron energy distribution functions in the neon positive column for [Ne] = 4×10^{18} cm^{-3}, $r = 0.15$ cm, and $T = 0.034$ eV ($p = 147$ torr). The Druyvestein distribution function is plotted for $y_0 = (6.2\ \text{eV})^2$.

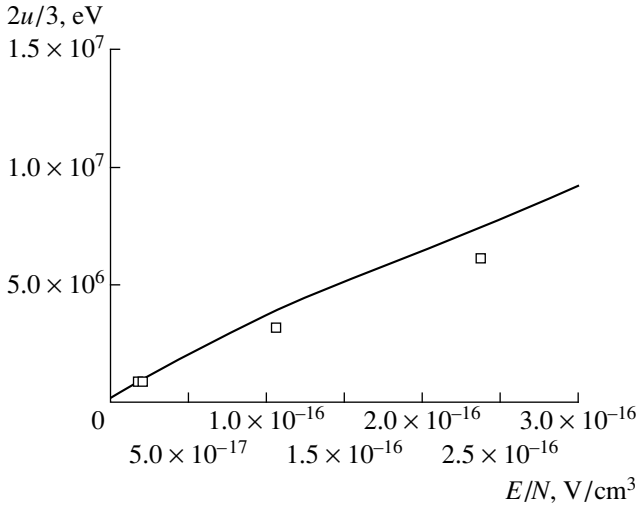

Fig. 3. Comparison of the calculated (dots) and experimental [59] (solid lines) dependences of the characteristic energy $2/3u$ on E_{st}/N, where E_{st} is the electric field strength corresponding to the steady-state discharge burning, N is the neon atomic density, ad u is the mean electron energy.

We represent this expression in the same way as in the previous section and obtain an expression similar to Eq. (5):

$$\exp(\beta^2 I^2/T_D^2)\left(\frac{I}{T_D}\right)^{3/2} = A(pr)^2, \qquad (8)$$

where

$$A = \frac{1}{\Gamma(3/4) \times 2.4^2 \beta^{5/2}}\left(\frac{I}{2m_e}\right)^{1/2}\frac{e\alpha}{\mu_+^0 N_0 \sqrt{T^3 T_0}}$$

and the relationship $p = NT$ is used. Figure 1 shows the dependence given by Eq. (8). For the gas temperature $T = 0.034$ eV (390 K), the coefficient A is calculated to be 1.707×10^3 (torr cm)$^{-1}$. In calculations for neon, we use $\alpha = 2.019 \times 10^{-18}$ cm^2/eV and the ion mobility $\mu_+^0 = 4.1$ cm^2/(V s). The latter value taken from [58] corresponds to a neon concentration of 2.69×10^{19} cm^{-3} and gas temperature $T = 300$ K.

Comparison with the results of calculations. In Fig. 1, dots show the results of simulation. In calculations, we set a pressure of 147 torr and numerically determine the electric field strength E of the positive column (see Section 2) and the corresponding electron temperature. The method of numerically determining the electron distribution function can be found in [51]. Based on the calculated distribution function, we numerically determine the mean electron energy, multiply it by a factor of 2/3, and obtain the electron temperature. To test the validity of expression (8), we perform calculations at a few values of the pressure and the discharge tube radius. It is seen that the results obtained are in good agreement with the curve built using the Druyvestein electron distribution function.

This agreement is related to the fact that the calculated distribution function virtually coincides with the Druyvestein function (Fig. 2). The reason for the difference in the range of the neon excitation energy is the fact that the Druyvestein distribution is derived with neglect of inelastic transitions.

The numerically calculated dependences of the characteristic energy T_D and the drift velocity v_D on E/N (N is the neon atomic density) are in good agreement with the experimental data from [59] (Figs. 3, 4).

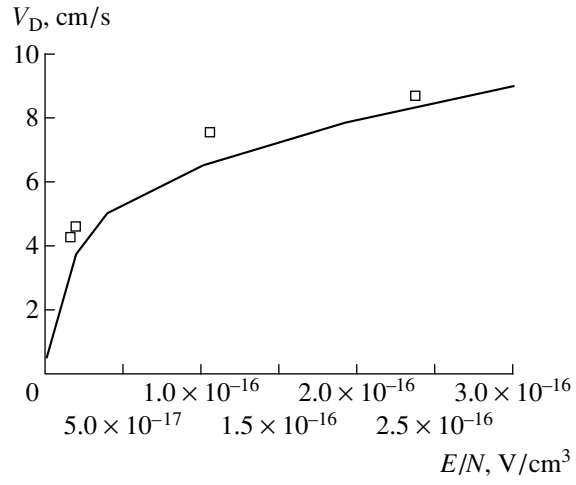

Fig. 4. Comparison of the calculated (dots) and experimental [59] (solid lines) dependences of the drift velocity v_D on E_{st}/N.

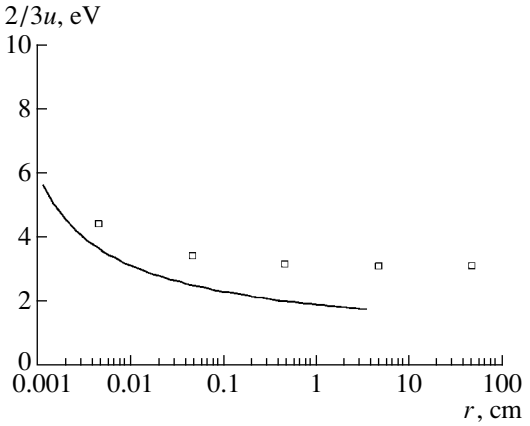

Fig. 5. Characteristic energy 2/3*u* vs. *pr* for the positive column of the krypton glow discharge. Solid line and dots correspond to the results obtained for the Druyvestein electron energy distribution function and the results of simulation, respectively. For simplicity, the curves are plotted for p = 14.7 torr.

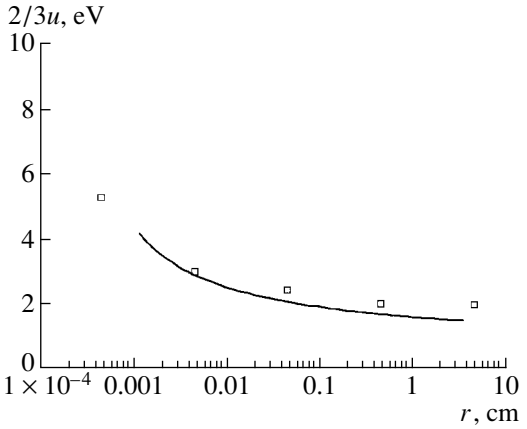

Fig. 6. Characteristic energy 2/3*u* vs. *pr* for the positive column of the xenon glow discharge. Solid line and dots correspond to the results obtained for the Druyvestein electron energy distribution function and the results of simulation, respectively. For simplicity, the curves are plotted for p = 14.7 torr.

Thus, the comparison of the results of test calculations and experimental data demonstrates the adequacy of the model for the case of glow discharge in pure neon.

Krypton and xenon. As in the case of neon, we perform simulation of the glow discharge and obtain the dependences of 2/3*u* on *pr* for pure krypton (Fig. 5) and xenon (Fig. 6). Note the presence of the Ramsauer minima in the cross sections of electron elastic scattering by heavy rare gases in the low-energy range. The corresponding electron distribution function can be different from the Druyvestein distribution function. Nevertheless, we obtain satisfactory agreement between the analytical result based on the Druyvestein distribution and the results of numerical calculations.

4. BINARY MIXTURES

The main pumping channels of exciplex molecules. In exciplex lasers, the emitting states of molecules are predominantly pumped by the ion–ion recombination of the rare gas positive ions and the halogen negative atomic ions [51]. The typical pressures of the glow-discharge exciplex lamps are about 10 torr. At such pressures, the emitting states of exciplex molecules are populated mainly owing to the harpooning reactions, whose rates for the major part of molecules range from 10^{-10} to 10^{-9} cm^3/s. The analysis of the kinetic processes that affect the emission of the mixture shows that the emitting states are predominantly populated owing to the excitation of the rare gas atomic states; for example,

$$\mathrm{Kr} + e \longrightarrow \mathrm{Kr}^* + e$$

$$\mathrm{Xe} + e \longrightarrow \mathrm{Xe}^* + e.$$

The harpooning reactions result in the populating of exciplex molecules:

$$\mathrm{Kr}^* + \mathrm{Cl}_2 \longrightarrow \mathrm{KrCl}^* + \mathrm{Cl}$$

$$\mathrm{Xe}^* + \mathrm{Cl}_2 \longrightarrow \mathrm{XeCl}^* + \mathrm{Cl}.$$

Table 1 shows the rates directly related to the formation and quenching of XeCl and KrCl molecules. Before we present the results of simulation, note a few features of the model.

The rates of harpooning reactions. In experiments, the total reaction rates are the most easy to measure; for example,

$$R^* + MX \longrightarrow \text{products}. \qquad \text{(A)}$$

Then, the total reaction rates can be specified for individual reaction channels. In particular, for $MX = \mathrm{Cl}_2$ and MX = HCl molecules, the total rates k_{tot} correspond to the harpooning reaction rate k_{harp} and the quenching rate k_{q} of the rare gas R excited states, respectively. In the latter case, it is difficult to determine the rates of the harpooning reactions. It is known from [60] that the rate $k_{\mathrm{harp}}(v = 1)$ of the reaction

$$\mathrm{Xe}^* + \mathrm{HCl}(v = 1) \longrightarrow \mathrm{XeCl}^* + \mathrm{H}$$

is greater than 2×10^{-10} cm^3/s (if the calculations employ $k_{\mathrm{harp}}(v = 0) = k_{\mathrm{harp}}(v = 1)$, the power and the emission efficiency differ from those obtained for the binary mixtures at $k_{\mathrm{harp}}(v = 0) = 0$ by more than two orders of magnitude). The rates of the harpooning reactions with the molecules in the ground vibrational state are low. For example, for the reaction

$$\mathrm{Kr}^* + \mathrm{HCl}(v = 0) \longrightarrow \mathrm{KrCl}^* + \mathrm{H},$$

the rate is 2.4×10^{-11} cm^3/s [61] and, for the reaction

$$\mathrm{Xe}^* + \mathrm{HCl}(v = 0) \longrightarrow \mathrm{XeCl}^* + \mathrm{H},$$

Table 1. Rates of the harpooning reactions and the quenching of exciplex molecules used in simulation of the glow discharge. In the expressions for the rates, the dimensionality of the gas temperature is electronvolts; n is the number of particles taking part in the reaction. In the case of three-particle reactions, we take into account the reverse rates related to the Saha–Boltzmann relationships. The rates of the harpooning reactions involving HCl are assumed to be equal to the total reaction rates (see Section 4)

No.	Reaction	Rate, cm^{3n}/s
1	$Kr^* + HCl\ (v = 0–2) \longrightarrow KrCl^* + H$	5×10^{-10}
2	$Kr^* + Cl_2 \longrightarrow KrCl^* + Cl$	7.3×10^{-10}
3	$Kr^* + Kr \longrightarrow 2Kr$	1.64×10^{-11}
4	$Kr^* + 2Kr \longrightarrow Kr_2^* + Kr$	7.3×10^{-32}
5	$Kr^* + Kr + Ne \longrightarrow Kr_2^* + Ne$	1×10^{-32}
6	$Kr^* + 2Ne \longrightarrow NeKr^* + Ne$	1×10^{-32}
7	$KrCl^* + HCl\ (v = 0–2) \longrightarrow Kr + Cl + H + Cl$	6×10^{-10}
8	$KrCl^* + Cl_2 \longrightarrow Kr + Cl + Cl_2$	6×10^{-10}
9	$KrCl^* + Kr \longrightarrow 2Kr + Cl$	5.4×10^{-12}
10	$KrCl^* + Kr + Ne \longrightarrow Kr_2Cl^* + Ne$	2×10^{-31}
11	$KrCl^* + Ne \longrightarrow Kr + Cl + Ne$	3×10^{-13}
12	$KrCl^* + 2Ne \longrightarrow NeKrCl^* + Ne$	1×10^{-32}
13	$Xe^* + HCl\ (v = 0–2) \longrightarrow XeCl^* + H$	2×10^{-10}
14	$Xe^* + Cl_2 \longrightarrow XeCl^* + Cl$	10^{-9}
15	$Xe^* + Xe \longrightarrow 2Xe$	3.5×10^{-15}
16	$Xe^* + 2Xe \longrightarrow Xe_2^* + Xe$	$5 \times 10^{-32}(T_g/0.026)^{-1/3}$
17	$Xe^* + Ne + Xe \longrightarrow Xe_2^* + Ne$	$1.2 \times 10^{-32}(T_g/0.026)^{-1/3}$
18	$Xe^* + 2Ne \longrightarrow NeXe^* + Ne$	$5 \times 10^{-34}(T_g/0.026)^{-1/3}$
19	$XeCl^* + HCl\ (v = 0–2) \longrightarrow XeCl(X) + H + Cl$	6.3×10^{-10}
20	$XeCl^* + Cl_2 \longrightarrow Xe + Cl + Cl_2$	6.3×10^{-10}
21	$XeCl^* + Xe \longrightarrow 2Xe + Cl$	3.2×10^{-12}
22	$XeCl^* + Xe + Ne \longrightarrow Xe_2Cl^* + Ne$	1.5×10^{-31}
23	$XeCl^* + Ne \longrightarrow Xe + Cl + Ne$	3.3×10^{-13}
24	$XeCl^* + 2Ne \longrightarrow Xe + Cl + 2Ne$	1×10^{-33}

the rate is less than 1×10^{-11} cm^3/s [62] or 7.2×10^{-12} cm^3/s [63]. There exist no theoretical calculations of these rates.

Structure of the results presented. Thus, the rates of the above reactions will be specified in future. To make the results of the calculations applicable, we assume that the reactions (A) have only one (harpooning) channel and the total reaction rates k_{tot} equal the rates k_{harp} of the corresponding harpooning reactions (the quenching rates equal zero). To obtain real values of the lamp power and efficiency, one must multiply the values from Tables 2 and 3 by the ratio k_{harp}/k_{tot}. The emission characteristics weakly vary with k_{harp} at $k_q = 0$ (see the analysis of the variation in the harpooning reaction rates given below). Therefore, in the case of a variation in both k_{harp} and k_{tot}, we still multiply the above values by the ratio k_{harp}/k_{tot}. In general, the quenching rate of xenon Xe* and krypton Kr* excited states by HCl molecule is about 5×10^{-10} cm^3/s. Thus, the data presented in the tables for the HCl molecule should be decreased by a factor of 20–30. The dependences of the efficiencies on the partial concentrations of chlorine-containing molecules are more flat than the dependences of the radiation power; so in a few cases the tables show a range of parameters in which the efficiency varies very weakly. As a rule, even in the cases when the tables show a single value, the efficiency

Table 2. (a) The optimum values of [HCl], power density P, and emission efficiency η of a glow-discharge lamp with a Kr/HCl binary mixture. In parentheses, we present the parameters corresponding to optimum efficiency. The preionization rate is 10^{-3} s^{-1}. The results presented are obtained under the assumption that reactions (A) have only one (harpooning) channel and the total rates k_{tot} of reactions (A) are equal to the harpooning reaction rates k_{harp}. To obtain real values of the power and emission efficiency, the values represented should be multiplied by the ratio k_{harp}/k_{tot} (see Section 4 for details)

	[HCl], cm^{-3}	P, W/cm^3	η, %
[Kr] = 4×10^{17} cm^{-3}			
r = 0.045 cm	2.5×10^{16}	1.25×10^{-1}	16.8
r = 0.45 cm	1×10^{16} (2.5×10^{16})	9.52×10^{-2} (5.03×10^{-2})	14.9 (15.4)
r = 4.5 cm	2.5×10^{16}	6.02×10^{-2}	15.4
[Kr] = 4×10^{18} cm^{-3}			
r = 0.045 cm	1×10^{17}	4.09×10^{-1}	4.92
r = 0.45 cm	5×10^{16} (1×10^{17})	5.80×10^{-1} (2.38×10^{-1})	4.45 (4.77)
r = 4.5 cm	5×10^{16} (1×10^{17})	5.99×10^{-1} (2.45×10^{-1})	4.46 (4.80)
[Kr] = 4×10^{19} cm^{-3}			
r = 0.45 cm	2×10^{18} (1×10^{18})	5.44×10^{-1} (4.37×10^{-1})	3.78×10^{-1} (4.37×10^{-1})

Table 2. (b) The optimum values of [Cl_2], power density P, and emission efficiency η of a glow-discharge lamp with a Kr/Cl_2 binary mixture. In parentheses, we present the parameters corresponding to optimum efficiency. The preionization rate is 10^{-3} s^{-1}

	[Cl_2], cm^{-3}	P, W/cm^3	η, %
[Kr] = 4×10^{17} cm^{-3}			
r = 0.045 cm	2.5×10^{16}	6.04×10^{-2}	22.8
r = 0.45 cm	1×10^{16} (2.5×10^{16})	1.29×10^{-2} (1.1×10^{-2})	21.6 (23.3)
r = 4.5 cm	1×10^{16} (2.5×10^{16})	2.03×10^{-3} (1.73×10^{-3})	21.5 (23.3)
[Kr] = 4×10^{18} cm^{-3}			
r = 0.045 cm	1×10^{17}	2.07×10^{-1}	7.09
r = 0.45 cm	1×10^{16} (1×10^{17})	1.13×10^{-1} (5.55×10^{-2})	2.71 (7.53)
r = 4.5 cm	1×10^{16} (1×10^{17})	2.76×10^{-1} (5.13×10^{-2})	2.82 (7.53)
[Kr] = 4×10^{19} cm^{-3}			
r = 0.45 cm	1×10^{17} (1×10^{18})	2.81×10^{-1} (9.43×10^{-2})	3.01×10^{-1} (6.62×10^{-1})

weakly varies with a 1.5- to 2-fold variation in the concentration of the molecules.

In calculations, the ionization rate equals 10^{-3} s^{-1} with duration about 10 μs. The radiation power linearly increases with the preionization rate.

The variation in the rates of the harpooning reactions and the quenching of the excited states R*. As was mentioned, the quenching rate k_q is assumed to be equal to zero. If we take into account nearly equal rates k_{harp} and k_q, the optimum with respect to HCl is virtually unshifted. When k_{harp} increases by a factor of 2–3 at k_q = 0, the lamp power and efficiency remain virtually unchanged. In particular, the increase in k_{harp} for HCl from 2×10^{-10} to 5×10^{-10} cm^3/s (reaction no. 12 in Table 1) leads to a 20% increase in the power and efficiency. This can be expected, since at typical electron concentrations (10^{10}–10^{11} cm^{-3}) the flow of the excited electron states of rare gases is intercepted by the harpooning reactions and the variation in the harpooning reaction rate leads to a variation in the concentration of the rare gas excited states rather than the flow.

The optimum concentration of halogen-containing molecules in the mixture. As was mentioned in Section 2, the models presented are based on the models used to describe exciplex lasers and lamps pumped by the barrier and volume pulsed discharges. However, when used to describe glow discharge, this model can produce erroneous data regarding the optimum composition of the mixture. This happens

Table 3. (a) The optimum values of [HCl], power density P, and emission efficiency η of a glow-discharge lamp with a Xe/HCl binary mixture. In parentheses, we present the parameters corresponding to optimum efficiency. The preionization rate is 10^{-3} s^{-1}. See heading of Table 2a for comments on real powers and efficiencies

	[HCl], cm^{-3}	P, W/cm^3	η, %
[Xe] = 4×10^{17} cm^{-3}			
r = 0.045 cm	5×10^{15} (1×10^{15})	2.41×10^{-1} (1.25×10^{-1})	35.1 (40.1)
r = 0.45 cm	2×10^{15}–5×10^{15}	1.18×10^{-1}	31.0
r = 4.5 cm	5×10^{15}	1.5×10^{-1}	32.2
[Xe] = 4×10^{18} cm^{-3}			
r = 0.045 cm	5×10^{16} (2.5×10^{16})	2.11 (1.87)	16.7 (19.3)
r = 0.45 cm	1×10^{16} (2.5×10^{16})	1.67 (1.61)	17.6 (19.3)
r = 4.5 cm	1×10^{16} (2.5×10^{16})	1.67 (1.60)	17.7 (19.4)
[Xe] = 4×10^{19} cm^{-3}			
r = 0.45 cm	1×10^{17} (4×10^{17})	8.08×10^{-1} (5.71×10^{-1})	6.92×10^{-1} (9.96×10^{-1})

Table 3. (b) The optimum values of [Cl_2], power density P, and emission efficiency η of a glow-discharge lamp with a Xe/Cl_2 binary mixture. In parentheses, we present the parameters corresponding to optimum efficiency. The preionization rate is 10^{-3} s^{-1}

	[Cl_2], cm^{-3}	P, W/cm^3	η, %
[Xe] = 4×10^{17} cm^{-3}			
r = 0.045 cm	1×10^{15} (5×10^{15}–5×10^{14})	2.45×10^{-1}	42.4
r = 0.45 cm	5×10^{14} (5×10^{15}–1×10^{15})	1.52×10^{-1} (1.07×10^{-1})	39.3 (42.6)
r = 4.5 cm	1×10^{15} (5×10^{15}–5×10^{14})	2.68×10^{-1}	42.6
[Xe] = 4×10^{18} cm^{-3}			
r = 0.045 cm	5×10^{15} (2.5×10^{16}–5×10^{15})	3.68 (2.62)	27.9 (28.8)
r = 0.45 cm	1×10^{16} (2.5×10^{16}–5×10^{15})	2.62	29.3
r = 4.5 cm	2.5×10^{16} (2.5×10^{16}–5×10^{15})	4.74 (2.48)	27.2 (29.2)
[Xe] = 4×10^{19} cm^{-3}			
r = 0.45 cm	1×10^{16} (1×10^{17}–2.5×10^{16})	8.34 (7.21)	1.90 (3.85)

because, in the aforementioned works, the main mechanism of the exciplex molecule pumping involves the ion–ion recombination reactions. In the glow discharge, the harpooning reactions play the key role. To prove the adequacy of the results obtained, it is needed to test the model using detailed experimental data. However, we know of only one experiment of this kind [39, 40].

At high currents in the glow discharge tubes, the emission efficiency of the mixtures containing Cl_2 molecules is significantly higher than that of the mixtures containing HCl molecules [39, 43] (note that the best characteristics of XeCl and KrCl exciplex lasers are obtained with the HCl molecule [51]). This is a consequence of the fact that the rates of the harpooning reactions with Cl_2 molecules are substantially higher than those with HCl molecules [39] (see also the section on the rates of the harpooning reactions). At low currents of the glow discharge, the emission efficiencies of the mixtures with these two donors of chlorine molecules are nearly equal [41, 43]. The aforementioned difference in the efficiencies cannot be related to the difference in the reaction rates. Supporting evidence for this is found in the equality of the emission efficiencies at low currents. On the other hand, the difference in the efficiencies at equal rates of the harpooning reactions can be caused by impurities. However, the effect of impurities should be independent of the glow discharge current.

A possible reason for this is the partial dissociation of the HCl molecule. When the discharge is switched on, the initial concentration of HCl molecules can differ from the real concentration of HCl molecules in the glow discharge plasma. In the plasma, HCl molecules dissociate (owing to the harpooning reactions yielding exciplex molecules) into H and Cl atoms and, at the

same time, these atoms associate into HCl and Cl_2 molecules. Thus, a working lamp initially containing only HCl molecules accumulates Cl_2 molecules, which accounts for the equality of the efficiencies. It is still unclear why this happens only at low currents.

In the case of significant dissociation of the molecules, the real concentrations of HCl and Cl_2 are always less than the initial concentrations of these molecules in the mixture. The rate of the volume association reaction

$$H(Cl) + Cl + Kr \longrightarrow HCl(Cl_2) + Kr$$

is low especially at low pressure of the mixture. It is possible that HCl and Cl_2 molecules are formed at the tube walls, but the rate of this process is unknown. Thus, we do not know the real degree of dissociation of HCl and Cl_2 molecules in the discharge. Therefore, we cannot directly compare the calculated optimum concentrations with the experimental data. Tables 2 and 3 show the concentrations of HCl and Cl_2 molecules that must be realized in the discharge (below, we use the same values). They are always less than the initial concentrations.

The results of calculations at high pressures. Computer codes do not calculate the discharge stability. Therefore, it is possible that the discharge with a positive column radius $r = 4.5$ cm and/or [Xe], [Kr] ~ 4×10^{19} cm^{-3} does not exist. Nevertheless, we present the results of calculations for these values. Note that, in experiments, it is easier to realize a discharge with a mixture pressure of about 10 torr, which corresponds to the lower bound concentration (about 4×10^{17} cm^{-3}) of the [Xe] and [Kr] concentration ranges.

Amplification. The ultimate ionization rate at which the discharge exists in calculations is about 10 s^{-1}. At such preionization rates, we do not perform a comparison with the experimental data. Taking into account the above consideration, we admit that such a discharge might be unrealizable. Nevertheless, the concentrations of exciplex molecules calculated at this preionization rate are no greater than 10^{11} cm^{-3} for a discharge pressure of 10 torr. In this case, the amplification of the active medium is too low to provide continuous generation of the exciplex molecules. A discussion of the problems related to the possibility of continuous generation of exciplex molecules in lamp sources can be found in [31, 32, 36]. In particular, the analysis of the glow discharge is presented in [36].

4.1. Kr/HCl and Kr/Cl_2 Mixtures

Optimum concentration of the mixture. For the binary mixtures, we perform optimization with respect to energy and emission efficiency. The concentrations of HCl corresponding to the optimum power and efficiency differ by a factor of no greater than two. The optimization employs three values of the tube radius and three values of the Kr concentration. The highest energy density of radiation corresponds to a krypton concentration [Kr] ~ 4×10^{18} cm^{-3} (Table 2). The energy density remains virtually unchanged with a further increase in the krypton concentration. When the concentration decreases from 4×10^{18} to 4×10^{17} cm^{-3}, the energy density decreases by an order of magnitude and the efficiency increases approximately four times. For the Cl_2 molecule, the difference between the optimum concentrations with respect to the power and efficiency and the variations in the optimum values of the power and efficiency substantially depend on the Kr concentration (pressure of the mixture) and the radius of the gas-discharge tube. Table 2 shows HCl and Cl_2 concentrations corresponding to the optimum values of the radiation power; the values in parentheses correspond to the optimum efficiency.

Preionization. The values of the power presented correspond to a preionization rate of 10^{-3} s^{-1}. As was mentioned, at this level, the power linearly increases with the preionization rate. Therefore, the most informative data are those regarding the calculated efficiencies. Different preionization levels in different experiments correspond to different current densities in the discharge tube.

4.2. Xe/HCl and Xe/Cl_2 Mixtures

Table 3 shows the data for xenon. As in the krypton-containing mixtures, the highest energy density corresponds to the concentration [Xe] ~ 4×10^{18} cm^{-3}. A further increase in the xenon concentration also does not lead to variations in the energy density. When the xenon concentration decreases from 4×10^{18} to 4×10^{17} cm^{-3}, the energy decreases by a factor of 10–20 and the efficiency increases by approximately 1.5 times.

5. TERNARY MIXTURES

Adding neon makes it possible to increase the lamp power. Let us consider this effect through the example of an Ne/Kr/Cl_2 ternary mixture using the lamp parameters from [64]. For the glow discharge in a 150-cm-long lamp with a Kr/Cl_2 binary mixture and a tube radius of 2.8 cm, the radiation power is 100 W. The corresponding power density is 3.38×10^{-2} W/cm^3. Nearly the same power density is realized in the calculations at the preionization rate $\nu = 3 \times 10^{-2}$ s^{-1} corresponding to neon.

5.1. Increase in the Concentration of Discharge Electrons

The results of calculations show that adding neon to the Kr/Cl_2 mixture leads to an increase in the electric field strength E_{st} of the positive column corresponding to the steady state (Fig. 7b). The value calculated is in good agreement with the experimentally measured electric field strength of 17 V/(cm torr). With neon added to the mixture, the mean energy of discharge electrons decreases. It may seem that this impedes the

excitation of the lower excited states of krypton in the reaction

$$Kr + e \longrightarrow Kr^* + e.$$

In reality, the concentration of these excited states increases owing to the growth of the concentration of electrons. The concentration of electrons increases with the electric field strength in the positive column. This accelerates the excitation reaction. The concentration of Kr* increases, and the contribution of the harpooning reaction to populating the emitting state of the exciplex molecule KrCl* grows. The consequences of this are an increase in the radiation power and a decrease in the efficiency. The latter is related to the growing contribution of the reactions in which neon atoms quench the emitting states (Fig. 7a).

The above mechanism corresponds to the case when neon is added to the mixture at a fixed concentration of krypton. The power increases with the electric field strength and, hence, the energy deposited into the discharge. What happens if the energy deposition is fixed?

5.2. Adding Neon at Fixed Energy Deposition

In calculations, the energy deposition varies with the ionization rate. When the neon concentration increases, the ionization rate varies in such a way that the product of the discharge current and the electric field strength remains unchanged. In calculations, we do not observe an increase in the radiation power either in the case of increasing neon concentration at a fixed krypton concentration or in the case of substituting neon for krypton at a constant total concentration of the mixture. Note that, in [64], adding neon at the fixed energy deposition into the active medium caused an increase in the lamp power. When small amounts (about 20% of the total pressure) of helium, neon, or argon are added to the original Kr/Cl_2 or Xe/Cl_2 mixture, the power and efficiency of the glow-discharge lamps increase. The best and the worst results are obtained with helium and argon added, respectively. Adding neon yields an intermediate increase.

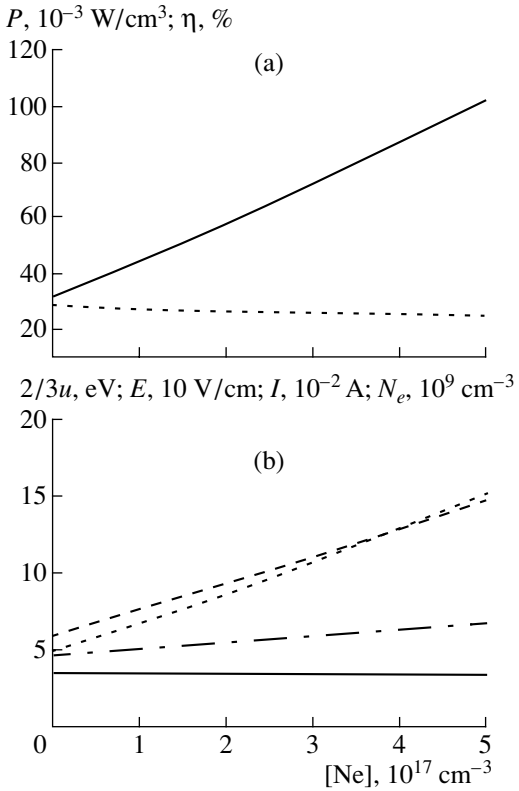

Fig. 7. (a) Power density P (solid line), emission efficiency η (dashed line), (b) $2/3u$ (u is the mean electron energy in the discharge) (solid line), electric field strength E of the positive column (dashed-and-dotted line), discharge tube current I (dotted line), and discharge electron concentration N_e (dashed line) vs. the concentration of neon added to the Kr/Cl_2 mixture for $[Kr] = 10^{17}$ cm^{-3}, $[Cl_2] = 2 \times 10^{16}$ cm^{-3}, preionization rate $\nu = 3 \times 10^{-2}$ s^{-1}, and discharge diameter $d = 56$ mm.

6. COMPARISON WITH EXPERIMENTS

A detailed study of XeCl and KrCl excimer lamps with Xe/Cl_2 and Kr/Cl_2 binary mixtures at various pressures and partial compositions of the mixture can be found in [39]. The tube radius is 1 cm. In experiments, the optimum ratios $[Xe]/[Cl_2]$ and $[Kr]/[Cl_2]$ are 50 : 1 and 30 : 1, respectively. These ratios are in agreement with the results of optimization (Tables 2b and 3b). However, the experimental curves of the power and efficiency are more sharp than the calculated ones in the vicinity of the optimum values.

The calculations employ the same preionization rate, $\nu = 10^{-3}$ s^{-1}, as the optimization of the mixtures (Tables 2, 3). The gas temperature of the active medium is 450 K. As was mentioned, the calculated power varies virtually linearly with the preionization rate. Therefore, the efficiencies and powers are compared in absolute and relative units, respectively.

Xe/Cl_2. For comparison with experimental data, we perform calculations at the concentration ratio $[Xe]/[Cl_2] = 50 : 1$. Figure 8 shows reasonable agreement between the experimental and calculated curves. The calculated efficiency is approximately 2.5 times greater than the theoretical one. Note that, in the experiments there was measured the voltage at the discharge tube rather than the field. For the purposes of comparison, we simply divide this voltage by the tube length. In the presence of a cathode voltage drop (not mentioned in [39]), the slope of the experimental curve decreases. This leads to better agreement with the results of calculations.

Kr/Cl_2. For comparison with experimental data, we perform the calculations at the concentration ratio $[Kr]/[Cl_2] = 30 : 1$. The agreement between the calculated and experimental characteristics is worse than in

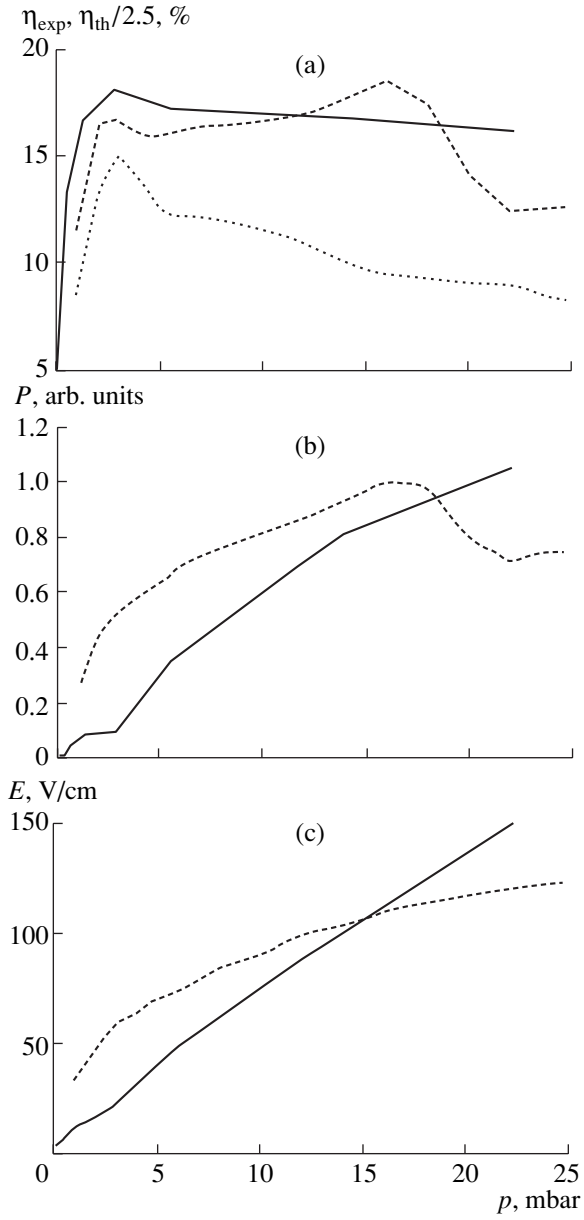

Fig. 8. (a) Efficiency, (b) power density, and (c) electric field strength of the positive column vs. pressure of the mixture: experimental results for $[Xe]/[Cl_2] = 40 : 1$ (dashed line) and 50 : 1 (dotted line) and the results of calculations for $[Xe]/[Cl_2] = 50 : 1$ (solid line).

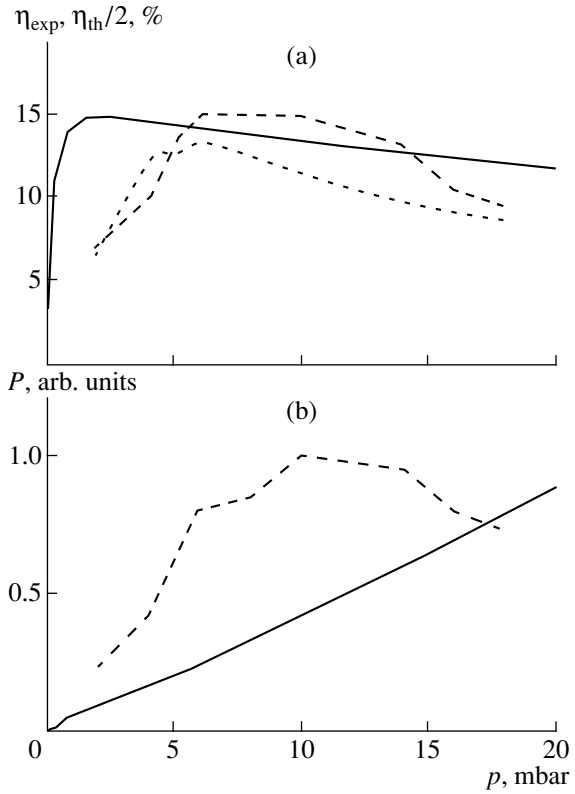

Fig. 9. (a) Efficiency and (b) power density vs. pressure of the mixture: experimental results (dotted line) and the results of calculations (solid line) for $[Kr]/[Cl_2] = 30 : 1$.

the case of the Xe/Cl_2 mixture (Fig. 9). The calculated efficiency is approximately two times greater than the theoretical one. The calculated dependence of the radiation power on the pressure is similar to that for the Xe/Cl_2 mixture. Note that the calculated current for the Xe/Cl_2 mixture remains virtually unchanged with a variation in pressure. For both mixtures, the experimental data are obtained at a constant current. In the calculations for the $KrCl_2$ mixture, the current monotonically increases with pressure, so that the slope of the theoretical curve in Fig. 9b must be decreased by approximately 1.5 times to make the comparison correct. However, this does not lead to significant changes in the results obtained.

6. CONCLUSIONS

We perform calculations of the emission characteristics of the glow-discharge KrCl (222 nm) and XeCl (308 nm) excimer lamps with binary (Kr and Xe with HCl and Cl_2) and ternary ($Ne/Kr/Cl_2$) mixtures.

To test the model, we compare, for neon, the calculated and experimental dependences of the characteristic energy and drift velocity of electrons on the ratio E_{st}/N of the electric field strength, corresponding to the steady-state discharge burning, to the concentration of the mixture. We demonstrate good agreement between the experimental and calculated values. The calculated dependences of the characteristic energy of electrons on the product pr of the pressure and the discharge radius coincide with the dependences obtained under the assumption of a Druyvestein electron velocity distribution function. The adequacy of the Druyvestein distribution function follows from the fact that the electron path in neon weakly depends on the electron energy.

The results of calculations show that under the optimum (with respect to efficiency) conditions the exciplex molecules are populated mainly owing to the harpooning reactions. This was mentioned in [41, 42].

The results of model calculations are compared to the experimental data from [39]. We obtain good agreement between the calculated and experimental dependences of the power, the emission efficiency, and the electric field strength of the positive column on the pressure of the Xe/Cl_2 mixture. For the Kr/Cl_2 mixture, the comparison yields worse agreement. The calculated optimum concentrations agree with the experimentally determined concentrations. The calculated power and emission efficiency weakly vary in the vicinity of the optimum concentration, whereas in experiments these quantities exhibit abrupt changes.

We optimize $Kr/HCl(Cl_2)$ and $Xe/HCl(Cl_2)$ binary mixtures. For krypton and xenon concentrations ranging from 4×10^{17} to 4×10^{18} cm^{-3}, the optimum (with respect to the power and emission efficiency) concentrations of HCl differ by a factor of no greater than 2 and range from 10^{16} to 10^{17} cm^{-3} for krypton-containing mixtures and from 2×10^{15} to 5×10^{16} cm^{-3} for xenon-containing mixtures. The corresponding optimum concentration of Cl_2 molecules can differ by an order of magnitude and range from 10^{16} to 10^{17} cm^{-3} for krypton-containing mixtures and from 5×10^{14} to 2.5×10^{16} cm^{-3} for xenon-containing mixtures. The variation in the total rate of reactions (A) does not lead to a variation in the optimum concentrations of the halogen-containing molecules.

In spite of a significant difference in the physical nature of HCl and Cl_2 molecules (different attachment cross sections, the processes of vibrational excitation, the dependences of the attachment cross section on the vibrational level of the molecule, etc.), the optimum (with respect to the emission efficiency) concentrations of these molecules are nearly equal.

The calculated emission efficiencies of the mixtures containing HCl and Cl_2 molecules could be equal provided the harpooning reaction rates for the former were not significantly less than those for the latter. In calculations, the emission efficiency for the KrCl(B) $\longrightarrow$ KrCl(X) (222 nm) transition at $[Kr] = 4 \times 10^{17}$ cm^{-3} can be as high as 15–20%. For $[Xe] = 4 \times 10^{17}$ cm^{-3}, the emission efficiency for the XeCl(B) $\longrightarrow$ XeCl(X) (308 nm) transition can reach 30–40%, which is close to the quantum limit of 40%. When the krypton concentration increases from 4×10^{17} to 4×10^{18} cm^{-3}, the efficiency decreases by approximately three times. The same increase in the xenon concentration leads to a 1.5-fold decrease in the efficiency.

Using the kinetic model for the $Ne/Kr/Cl_2$ mixture, we study the effect of adding neon on the radiation power and emission efficiency of KrCl* molecules.

The results of calculations show that the radiation power monotonically (nearly linearly) increases with the concentration of neon in a wide range of additionally increased neon concentration. This is related to the increase in the electric field strength of the positive column. In this case, the emission efficiency decreases, since the quenching of the emitting molecules increases with the concentration of neon. When the concentrations of neon and krypton are equal, the power increases by 40% in comparison with the level characteristic of a neon-free mixture. The calculated radiation power does not grow when neon is added under fixed energy deposition.

ACKNOWLEDGMENTS

This work was supported by the International Science and Technology Center, project no. 1270.

REFERENCES

1. E. N. Pavlovskaya, I. V. Podmoshenskiĭ, and A. V. Yakovleva, Zh. Prikl. Spektrosk. **20**, 504 (1974).
2. E. N. Pavlovskaya and A. V. Yakovleva, Opt. Spektrosk. **54**, 226 (1983).
3. B. Eliasson and U. Kogelschatz, Appl. Phys. B **46**, 299 (1988).
4. U. Kogelschatz and H. Esron, Laser Optoelektron. **22**, 55 (1990).
5. A. M. Boichenko, V. S. Skakun, V. F. Tarasenko, *et al.*, Laser Phys. **4**, 635 (1994).
6. F. Vollkommer and L. Hitzscke, in *Proceedings of 8th International Symposium on the Science and Technology of Light Sources*, Ed. by G. Babucke (Greifswald, 1998), p. 51.
7. A. M. Boichenko, V. S. Skakun, E. A. Sosnin, *et al.*, Laser Phys. **10**, 540 (2000).
8. R. P. Mildren and R. J. Carman, J. Phys. D **34**, L1 (2001).
9. A. M. Boichenko, V. S. Skakun, V. F. Tarasenko, *et al.*, Laser Phys. **3**, 834 (1993).
10. H. Kumagai and M. Obara, IEEE Trans. Plasma Sci. **16**, 453 (1988).
11. A. M. Boichenko, V. F. Tarasenko, and S. I. Yakovlenko, Laser Phys. **5**, 727 (1995).
12. A. M. Boichenko, V. S. Skakun, E. A. Sosnin, *et al.*, Kvantovaya Élektron. (Moscow) **23**, 344 (1996) [Quantum Electron. **26**, 336 (1996)].
13. D. J. Eckstrom, H. H. Nakano, D. C. Lorents, *et al.*, J. Appl. Phys. **64**, 1679 (1988).
14. D. J. Eckstrom, H. H. Nakano, D. C. Lorents, *et al.*, J. Appl. Phys. **64**, 1691 (1988).
15. J. Wieser, D. E. Murnick, A. Ulrich, *et al.*, Rev. Sci. Instrum. **68**, 1360 (1997).
16. A. M. Boichenko, Kvantovaya Élektron. (Moscow) **29**, 163 (1999) [Quantum Electron. **29**, 1001 (1999)].
17. A. M. Boichenko, S. I. Yakovlenko, and V. F. Tarasenko, Laser Part. Beams **18**, 655 (2000).
18. M. I. Lomaev, V. F. Tarasenko, and D. V. Shitts, Pis'ma Zh. Tekh. Fiz. **25** (21), 27 (1999).
19. V. F. Tarasenko, E. B. Chernov, M. V. Erofeev, *et al.*, Appl. Phys. A **69**, S327 (1999).

20. M. V. Erofeev, M. I. Lomaev, E. A. Sosnin, *et al.*, Opt. Zh. **68** (10), 75 (2001).
21. G. V. Runev and V. B. Saenko, Pis'ma Zh. Tekh. Fiz. **19**, 53 (1993).
22. H. Kumagai and M. Obara, Appl. Phys. Lett. **54**, 2619 (1989).
23. H. Kumagai and M. Obara, Appl. Phys. Lett. **55**, 1583 (1989).
24. H. Kumagai and M. Obara, Jpn. J. Appl. Phys. **28**, L2228 (1989).
25. I. Nakamura, F. Kannari, and M. Obara, Appl. Phys. Lett. **57**, 2057 (1990).
26. H. Kumagai and K. Toyoda, Appl. Phys. Lett. **59**, 2811 (1991).
27. A. E. Voitenko, E. P. Matochkin, and A. F. Fedulov, Prib. Tekh. Éksp., No. 2, 201 (1970).
28. M. A. Tsikulin and E. G. Popov, *Radiative Properties of Shock Waves in Gases* (Nauka, Moscow, 1977) (in Russian).
29. A. M. Boichenko, A. V. Karelin, and S. I. Yakovlenko, Laser Phys. **9**, 1190 (1999).
30. F. Sato, Y. Sunada, S. Okamoto, and F. Kannari, Appl. Phys. Lett. **61**, 1378 (1992).
31. A. A. Alekhin, V. A. Barinov, Yu. V. Geras'ko, *et al.*, Zh. Tekh. Fiz. **63** (2), 43 (1993).
32. A. A. Alekhin, V. A. Barinov, Yu. V. Geras'ko, *et al.*, Zh. Tekh. Fiz. **65** (5), 9 (1995).
33. A. P. Golovinskiĭ, Pis'ma Zh. Tekh. Fiz. **24** (6), 63 (1998).
34. A. Skudra, in *High Frequency Electrodeless Discharge Light Sources* (Acta Univ. Latvia, Riga, 1992), p. 67.
35. V. T. Mikhel'son, A. B. Treshchalov, V. A. Peet, *et al.*, Kvantovaya Élektron. (Moscow) **14**, 1404 (1987).
36. R. S. Taylor, K. E. Leopold, and K. O. Tan, Appl. Phys. Lett. **59**, 525 (1991).
37. A. P. Golovitskiĭ, Pis'ma Zh. Tekh. Fiz. **18** (8), 73 (1992).
38. A. P. Golovitskiĭ and S. N. Kan, Opt. Spektrosk. **75**, 604 (1993).
39. A. Schwabedissen and W. Botticher, Contrib. Plasma Phys. **35**, 517 (1995).
40. K. Tiedtke, A. Schwabedissen, G. Schroder, and W. Botticher, Contrib. Plasma Phys. **35**, 537 (1995).
41. A. M. Boichenko, A. N. Panchenko, V. F. Tarasenko, and S. I. Yakovlenko, Laser Phys. **5**, 1112 (1995).
42. A. M. Boichenko, A. N. Panchenko, V. F. Tarasenko, and S. I. Yakovlenko, Kvantovaya Élektron. (Moscow) **23**, 417 (1996) [Quantum Electron. **26**, 407 (1996)].
43. M. I. Lomaev, A. N. Panchenko, V. S. Skakun, *et al.*, Opt. Atmos. Okeana **9**, 199 (1996).
44. V. F. Tarasenko, M. I. Lomaev, D. V. Shitz, and V. S. Skakun, Proc. SPIE **4747**, 419 (2002).
45. A. N. Panchenko, E. A. Sosnin, V. S. Skakun, *et al.*, Pis'ma Zh. Tekh. Fiz. **21** (21), 77 (1995).
46. M. I. Lomaev, A. N. Panchenko, E. A. Sosnin, and V. F. Tarasenko, Zh. Tekh. Fiz. **68** (2), 64 (1998).
47. A. N. Panchenko, E. A. Sosnin, and V. F. Tarasenko, Opt. Commun. **161**, 249 (1999).
48. V. S. Skakun, M. I. Lomaev, V. F. Tarasenko, and D. V. Shitts, Pis'ma Zh. Tekh. Fiz. **28** (21), 42 (2002).
49. A. M. Boichenko, V. I. Derzhiev, A. G. Zhidkov, and S. I. Yakovlenko, Kvantovaya Élektron. (Moscow) **16**, 278 (1989) [Sov. J. Quantum Electron. **19**, 182 (1989)].
50. A. M. Boichenko and S. I. Yakovlenko, Kvantovaya Élektron. (Moscow) **21**, 253 (1994) [Quantum Electron. **24**, 236 (1994)].
51. A. M. Boichenko, V. F. Tarasenko, and S. I. Yakovlenko, Laser Phys. **10**, 1159 (2000).
52. Tr. Inst. Obshch. Fiz., Akad. Nauk USSR, Ed. by S. I. Yakovlenko (1989), Vol. 21.
53. Yu. P. Raĭzer, *The Physics of Gas Discharge* (Nauka, Moscow, 1987) (in Russian).
54. L. B. Loed, *Fundamental Processes of Electrical Discharges in Gases* (Wiley, New York, 1939).
55. A. Von Engel, *Ionized Gases* (Clarendon Press, Oxford, 1955).
56. H. S. W. Massey and E. H. S. Burhop, *Electronic and Ionic Impact Phenomena* (Clarendon Press, Oxford, 1952).
57. *Handbook of Mathematical Functions*, Ed. by M. Abramowitz and I. A. Stegun (Dover, New York, 1979).
58. B. M. Smirnov, *Physics of Weakly Ionized Gases* (Nauka, Moscow, 1978) (in Russian).
59. *Physical Quantities. Handbook*, Ed. by I. S. Grigor'ev and E. Z. Meĭlikhov (Énergoatoizdat, Moscow, 1991) (in Russian).
60. R. S. F. Chang, J. Chem. Phys. **76**, 2943 (1982).
61. M. T. Jones, T. D. Dreiling, D. W. Setser, and R. N. McDonald, J. Phys. Chem. **89**, 450 (1985).
62. J. H. Kolts, J. E. Velazco, and D. W. Setser, J. Chem. Phys. **71**, 1247 (1979).
63. H. C. Brashears, Jr. and D. W. Setser, J. Phys. Chem. **84**, 224 (1980).
64. A. N. Panchenko, E. A. Sosnin, and V. F. Tarasenko, RF Patent No. 2,089,962 (1995); Byull. Izobret., No. 25, 350 (1997).